JACC Vol. 30, No. 5
November 1, 1997:1360–7

Automatic Quantitation of Regional Myocardial Wall Motion and Thickening From Gated Technetium-99m Sestamibi Myocardial Perfusion Single-Photon Emission Computed Tomography

GUIDO GERMANO, PHD,*† JACOB EREL, MD,*† HOWARD LEWIN, MD,*†
PAUL B. KAVANAGH, MS,* DANIEL S. BERMAN, MD, FACC*†

Los Angeles, California

Objectives. **We developed an automatic quantitative algorithm for the measurement of regional myocardial wall motion and wall thickening from three-dimensional gated technetium-99m sestamibi myocardial perfusion single-photon emission computed tomographic images.**

Background. **The algorithm measures the motion of the three-dimensional endocardial surface using a modification of the centerline method, as well as wall thickening using both geometry (gaussian fit) and partial volume (counts).**

Methods. **The algorithm was tested using a "variable thickness" heart phantom, and the quantitative results were compared with visual segmental assessment of myocardial motion and thickening in 79 clinical patients with a wide range of ejection fractions (6% to 87%).**

Results. **Phantom measurements of simulated motion and thickening were accurate regardless of the camera used (dual or triple detector), the angular span of reconstructed data (180° or 360°), the amount of motion (3 or 6 mm) or the amount of thickening (33%, 50% or 100%). Quantitative measurements of segmental motion and thickening in the patients were correlated with visual scores (r = 0.668, exact agreement 72.6%, kappa 0.433 and r = 0.550, exact agreement 74.7%, kappa 0.408, respectively). Significant inverse linear relations exist between the global (summed) visual motion score and the average quantitative motion, and between the global (summed) visual thickening score and the average quantitative thickening. Automatic quantitative ejection fraction measurements correlated extremely well with average quantitative motion (r = 0.929) and thickening (r = 0.959).**

Conclusions. **Our algorithm is accurate and may be the first automatic technique for the quantitative three-dimensional assessment of regional ventricular function in cardiology.**

(J Am Coll Cardiol 1997;30:1360–7)

Assessment of left ventricular (LV) regional wall motion or regional wall thickening is an integral part of the clinical assessment of coronary artery disease as well as other cardiac diseases, and determinations of the extent and severity of functional abnormalities strongly predict subsequent clinical outcomes (1,2). Traditionally, assessment of regional function is made by expert visual evaluation of a two-dimensional data set derived from one of a wide variety of techniques, including contrast ventriculography (3), radionuclide ventriculography (4), echocardiography (5), magnetic resonance imaging (MRI) (6) and ultrafast computed tomography (7). Although quantitative methods for assessing regional wall motion and wall thickening have been derived, at times quite elaborate, none of these methods is completely automatic and none have reached widespread, practical clinical application. Also, on a practical basis, none of the routine clinical methods allows a truly three-dimensional assessment of regional ventricular function.

We recently developed an automatic method for defining endocardial boundaries of the heart throughout the cardiac cycle from gated myocardial perfusion single-photon emission computed tomographic (SPECT) images, and we validated the technique as accurate for measuring left ventricular ejection fraction (LVEF) (8) against first-pass measurements. The goal of the present study was to further test this automatic algorithm for the assessment of regional wall motion and regional wall thickening of the LV in comparison with expert visual analysis of gated technetium-99m (Tc-99m) sestamibi myocardial perfusion SPECT data.

Methods

Algorithms. We previously described the algorithms that automatically determine three-dimensional endocardial and epicardial surfaces from gated (8) and ungated (9) SPECT image data sets. In brief, for each interval of a gated SPECT

From the *Divisions of Medical Physics and Imaging and Cardiology, Department of Medicine and Division of Nuclear Medicine, Department of Imaging, Cedars-Sinai Research Institute, Cedars-Sinai Medical Center; and †Department of Radiological Sciences and Department of Medicine, University of California Los Angeles School of Medicine, Los Angeles, California. This work was supported in part by a Biomedical Engineering Research Grant from the Whitaker Foundation, Rosslyn, Virginia.

Manuscript received December 26, 1996; revised manuscript received June 26, 1997, accepted July 10, 1997.

Address for correspondence: Dr. Guido Germano, Division of Nuclear Medicine, Cedars-Sinai Medical Center, A047 North Tower LL, 8700 Beverly Boulevard, Los Angeles, California 90048. E-mail: germano@csmc.edu.

Published by Elsevier Science Inc.

0735-1097/97/$17.00
PII S0735-1097(97)00276-3

Abbreviations and Acronyms

LEHR = low energy, high resolution
LPO = left posterior oblique
LV = left ventricle, left ventricular
LVEF = left ventricular ejection fraction
MMS = midmyocardial surface
MRI = magnetic resonance imaging
RAO = right anterior oblique
SPECT = single-photon emission computed tomography (tomographic)
Tc-99m = technetium-99m
Tl-201 = thallium-201

study, a maximal count midmyocardial surface (MMS) is determined; then rays are subtended normally to it, and a count profile is extracted for each ray. An asymmetric gaussian is fitted to each profile, and the endocardial and epicardial points along that ray are taken to be located at a distance from the MMS equal to a given percentage of the inner and outer SDs of the gaussian, respectively. The SDs measured from count profiles with peaks falling below 50% of the maximal myocardial count in that interval are labeled as invalid and replaced with SDs that minimize the sum of the absolute differences between each invalid SD and the SD of each of its four spatially closest neighbors. In essence, contours are generated even in the apparent absence of perfusion by maximizing the smoothness of the surface patch defined by the invalid points, as demonstrated in patients with coronary artery disease (8,10).

The myocardial volume of the first gating interval (bound by the epicardial and endocardial surfaces as well as by the valve plane) is computed, and the myocardial volume of each subsequent interval is set equal to that of the first by adding appropriately scaled inner and outer corrective surfaces to the epicardial and endocardial surfaces determined for that specific later interval. The length $L_0[t, i]$ contributed, along profile i, to the unscaled corrective surfaces for interval t depends on the MMS pixel count along that profile in the first interval (generally representative of end-diastole) and the tth interval, as well as on the highest MMS pixel count over the entire myocardium in the first interval. In particular, a first corrective ratio δ is computed as the MMS pixel count along ray i in interval t divided by the MMS pixel count along the same ray in interval 1, this ratio being limited to a range between 0.5 and 2.0. Then, a weighting ratio α is calculated from the first interval data as the MMS pixel count along ray i divided by the highest MMS pixel count in the myocardium. The two variables α and δ are combined as shown in the following equations:

$$L_0[t, i] = (1 - \alpha) + \alpha\delta, \quad [1]$$

where

$$\alpha = \frac{\mathrm{MMS}[1, i]}{\max(\mathrm{MMS}[1, \mathrm{all}])}, \quad [2]$$

$$\delta = \frac{\mathrm{MMS}[t, i]}{\mathrm{MMS}[1, i]}, \quad [3]$$

and δ is set to 0.5 and 2.0 if the ratio in equation 3 is <0.5 or >2.0, respectively. The length $L[t, i]$ contributed, along profile i, to the *scaled* corrective surfaces for interval t is then

$$L[t, i] = L_0[t, i]\gamma[t], \quad [4]$$

where γ is the scaling factor necessary to make the myocardial volume of interval t equal to that of interval 1. On the basis of this determination of endocardial and epicardial surfaces, myocardial thickness, measured as the distance between those surfaces, takes into account both geometric and count (partial volume [11,12]) considerations, in gated files. Myocardial thickening is computed as the variation in thickness between end-diastole and end-systole and is expressed as the percent increase from diastolic thickness.

Regional motion is measured as the distance between a given point of the endocardial surface at end-diastole and end-systole. This distance is expressed in absolute terms (mm) and measured perpendicularly to the average MMS between end-diastole and end-systole—a modification of the "centerline" method (13), similar to that previously reported by Faber et al. (14). Left ventricular ejection fractions are derived from LV cavity volumes at end-diastole and end-systole, as derived in our previous study (8). The entire, totally automatic process starting with the gated short-axis data sets executes in ~20 s (<2 min if automatic reconstruction and reorientation is included, similarly to [15]) on a SunSPARC5 computer with 32 megabytes of RAM and no dedicated or proprietary hardware. The software is modular, written in the C language and utilizes the X-Windows graphic user interface and the OSF-Motif toolkit, making it easily portable within the Unix environment. In previously published validation studies, high agreement was demonstrated between rest LVEFs measured automatically from gated Tc-99m sestamibi SPECT and semiautomatically from gated equilibrium blood pool ventriculography (10) and first-pass measurements (8).

Chest phantom. To evaluate the algorithms' accuracy in measuring myocardial thickness, myocardial thickening and endocardial motion, a chest phantom was used (16). This lucite phantom consists of a 20 × 35-cm elliptical chamber containing two 10-cm diameter cylinders filled with silicon foam (to simulate the lungs) and a centrally located heart chamber. The heart chamber consists of an external 7.5-cm diameter cylinder containing three smaller cylinders with diameters of 5.0, 5.6 and 6.2 cm to simulate myocardial thicknesses of 0.6, 0.9 and 1.2 cm (Fig. 1). The LV cavity (internal portion of the three stacked and communicating cylinders) and the elliptical chest cavity were filled with water, whereas the "myocardium" (space between the external and three internal cylinders) was filled with water containing 6 mCi of Tc-99m. The phantom was imaged on a triple-detector camera (Prism 3000, Picker) using low energy, high resolution (LEHR) collimation, continuous detector rotation, 3° projections over 360° and 20 s of data collection per projection. The projection data were prefiltered with the standard two-dimensional Butterworth filter used in clinical practice for static Tc-99m sestamibi SPECT imaging (order 2.5, critical frequency 0.31 cycles/pixel, pixel size

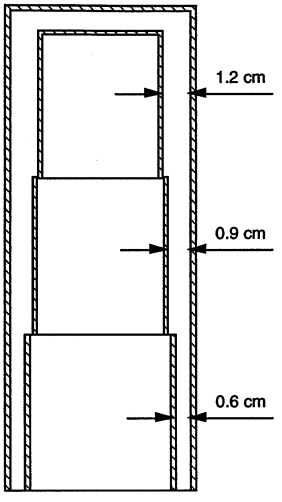

Figure 1. Longitudinal section of the heart chamber contained in the chest phantom.

0.53 cm for our system setup). Then, the projection data set was reconstructed over both 180° (45° right anterior oblique [RAO] to left posterior oblique projections [LPO]) and 360°, with filtered backprojection (ramp filter) and no attenuation correction. The phantom was also imaged on a dual-detector camera (Vertex, ADAC Laboratories) using LEHR collimation, pseudocontinuous detector rotation, 64 projections over 180° and 20 s of data collection per projection. The projection data were prefiltered (two-dimensional Butterworth, order 2.5, critical frequency 0.30 cycles/pixel, pixel size 0.64 cm) and reconstructed over 180° (45° RAO to LPO), with filtered backprojection (ramp filter) and no attenuation correction.

The previously described algorithms (8) that automatically determine three-dimensional endocardial and epicardial surfaces from SPECT image data sets were used to determine two-dimensional endocardial and epicardial contours from individual tomographic slices of the phantom data. For each slice, myocardial thickness was measured as the distance between the endocardial and epicardial contours, averaged over 36 equally spaced (10° apart) count profile rays. Myocardial thickening of 33%, 50% and 100% was simulated by taking a 0.9-, 0.6- and 1.2-cm slice as end-diastole, and a 1.2-, 0.9- and 1.2-cm slice as end-systole, respectively. Similarly, endocardial motion of 0.3 and 0.6 cm was simulated by taking a 0.6-cm slice as end-diastole and a 0.9- and 1.2-cm slice as end-systole, respectively. When measuring motion and thickening, a constraint similar to that of "constant myocardial volume" reported in our previous report (8) was introduced by ensuring that the myocardial area of a 0.9- and a 1.2-cm slice be 1.273 and 1.826 times that of a 0.6-cm slice, respectively. Finally, myocardial motion and thickening of 0% were simulated by taking two separate 1.2-cm slices as end-diastole and end-systole.

Clinical testing. In this prospective study, gated images were acquired from 79 randomly selected clinical patients (55 men, age 65 ± 12 years, weight 164 ± 35 lb, 15 with a previous myocardial infarction) undergoing a rest thallium-201 (Tl-201)/stress Tc-99m sestamibi "separate acquisition dual-isotope" gated SPECT protocol (17). In this protocol, injection of 3 to 3.5 mCi of Tl-201 is followed by Tl-201 SPECT imaging, which is then followed by injection of 25 to 30 mCi of Tc-99m sestamibi at peak stress and gated SPECT imaging 15 to 30 min later (treadmill exercise, n = 56) or 1 h later (pharmacologic stress using adenosine, n = 23).

All patient studies were acquired on a dual-detector camera (Vertex, ADAC) with the detectors oriented at 90°. The camera used LEHR collimation, step-and-shoot detector rotation, 64 projections over 180° (45° RAO to LPO) and 25 s of data collection per projection, distributed over eight cardiac frames. The acceptance window for cardiac cycle length was set to its maximal value of 100%, resulting in the acceptance of all counts from cardiac cycles with a duration within ±50% of the average, for each individual patient. The projection data sets were prefiltered with a two-dimensional Butterworth filter (order 5 and critical frequency 0.25 cycles/pixel, pixel size 0.64 cm) and reconstructed with filtered backprojection (ramp filter) and no attenuation correction. The resulting transaxial image sets were reoriented into short-axis sets, to which our automatic algorithm measuring myocardial wall motion and wall thickening was applied.

Semiquantitative visual assessment of regional (segmental) wall motion and wall thickening in the 79 gated Tc-99m sestamibi SPECT clinical studies was based on consensus of two experts (D.B., J.E.) who had no knowledge of the algorithm's quantitative results, and included a total of 20 LV segments, including six evenly spaced segments in each of an apical, midventricular and basal short-axis slice and two apical segments in a midventricular vertical long-axis slice, as previously described (17). The myocardial slices chosen for analysis were automatically assigned by the quantitative software. The gated Tc-99m sestamibi SPECT images were read in cinematic mode, using a "smoothed" cinematic display routine that performs real-time 3-point temporal interpolation of the images (kernel 0.5, 1.0 and 0.5) to reduce noise. Wall motion was scored on a 6-point scale (0 = normal; 1 = mild hypokinesia; 2 = moderate hypokinesia; 3 = severe hypokinesia; 4 = akinesia; 5 = dyskinesia) in the 20 segments described earlier. Wall thickening was scored on a 5-point scale (0 = normal; 1 = mildly impaired; 2 = moderately impaired; 3 = severely impaired thickening; 4 = absent thickening) based on the visual assessment of myocardial wall brightening from diastole to systole (11) in the same 20 segments. Unlike standard clinical reading, in which motion and thickening estimates are correlated and combined with perfusion assessment to yield a coherent final interpretation serving a diagnostic or prognostic goal, in this study assessment of motion and thickening was conducted independently and with the primary goal of comparing it with the automatic software assessment. Thus, visual scoring of wall motion was based exclusively on endocardial motion and used a 256-tone gray scale. Visual scoring of wall thickening was based on the brightening of the entire myocardium, and used both the 256-tone gray scale and a 10-step

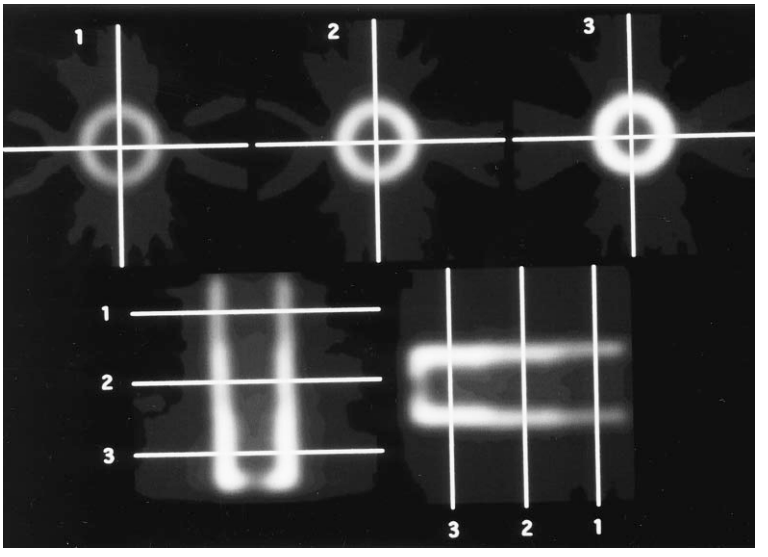

Figure 2. Top row, Short-axis slices corresponding to the thinner **(1),** average **(2)** and thicker **(3)** sections of the myocardial phantom. **Bottom row,** "Midventricular" horizontal **(left)** and vertical **(right)** long-axis sections of the same phantom.

color scale. In the case of perceived absent radionuclide uptake in a segment, that segment was, by definition, defined to be akinetic.

Correlation between quantitative and visual segmental function was performed by first extracting motion and thickening circumferential profiles from the end-diastolic and end-systolic images of each patient, and combining such profiles in "raw" motion and thickening polar maps similar to those previously described for perfusion analysis (18,19). Then, both polar maps were divided into 20 sections corresponding to the same six basal, six midventricular, six apical short-axis and two apical long-axis segments used for visual assessment, and the average quantitative motion and thickening in each section were calculated (20). In addition to this segmental assessment, visual estimates of global myocardial motion and thickening were derived in each patient by summing the 20 individual motion and the 20 individual thickening scores, respectively. These global motion and thickening scores were each grouped in four categories corresponding to values of 0 to 3, 4 to 8, 9 to 13 and >13, as previously proposed (9,21), then compared with the average quantitative motion (mm) and the average quantitative thickening (percent diastolic thickness) measured by the automatic algorithm. Average quantitative motion and thickening were finally compared to global quantitative LVEF.

Statistical analysis. Continuous variables are expressed as mean value ± SD. Average quantitative motion and thickening measurements corresponding to categoric variables were compared using one-way analysis of variance with multiple comparison (Bonferroni) correction, with $p < 0.05$ representing statistical significance. The agreement between quantitative LVEF and average motion, as well as that between quantitative LVEF and average thickening, was assessed using linear regression analysis (Pearson correlation coefficient). Agreement tables were evaluated using the unweighted kappa statistics, with $p < 0.05$ considered statistically significant. Kappa values <0.4, between 0.4 and 0.75 and >0.75 were taken to represent poor, fair to good and excellent agreement, respectively, based on Fleiss's classification (22).

Results

Phantom experiments. Figure 2 shows three short-axis (top row) and two long-axis images of the chest phantom, acquired using the triple-detector camera and reconstructed over 360°. The three short-axis slices shown (left to right: 6, 9 and 12 mm thick) are those used by the automated algorithm for measurements of thickness. Table 1 shows that initially measured myocardial thickness does not accurately reflect actual thickness, because the algorithm is designed to provide a linear but not a unitary slope relation between measured and actual thickness, even in the presence of a partial volume effect. Once

Table 1. Quantitative Measurements of Wall Thickness, Simulated Wall Motion and Simulated Wall Thickening Using the Variable Thickness Heart Phantom

	Triple Detector: 360°	Triple Detector: 180°	Dual Detector: 180°
Thickness			
6 mm	10.66 ± 0.43	10.59 ± 0.71	10.36 ± 0.83
9 mm	10.88 ± 0.42	10.85 ± 0.66	10.61 ± 0.89
12 mm	11.22 ± 0.37	11.13 ± 0.66	10.81 ± 0.82
Thickening			
1.00 (0%)	1.00 ± 0.04	1.01 ± 0.07	1.00 ± 0.09
1.33 (33%)	1.32 ± 0.07	1.34 ± 0.12	1.33 ± 0.15
1.50 (50%)	1.53 ± 0.08	1.52 ± 0.13	1.53 ± 0.17
2.00 (100%)	2.02 ± 0.10	2.04 ± 0.18	2.03 ± 0.22
Motion			
0 mm	0.01 ± 0.06	0.02 ± 0.10	0.01 ± 0.21
3 mm	2.73 ± 0.14	2.74 ± 0.19	2.66 ± 0.44
6 mm	5.45 ± 0.22	5.47 ± 0.28	5.32 ± 0.67

Data presented are mean value ± SD.

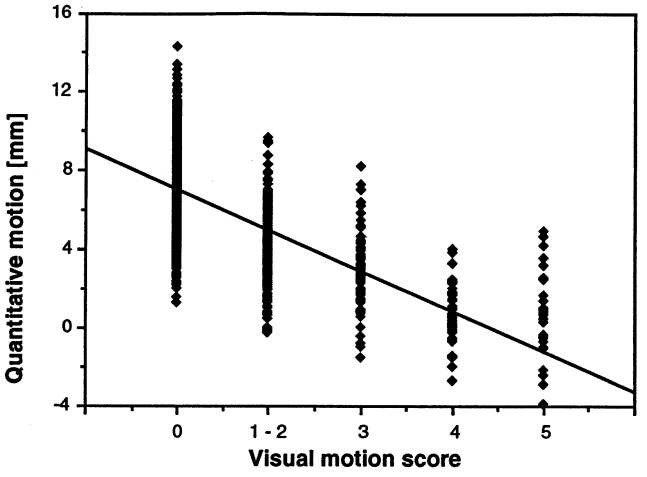

Figure 3. Quantitative segmental motion versus visual motion scores in the 1,125, 139, 156, 82, 43 and 35 segments (total 1,580) with visual motion scores of 0, 1, 2, 3, 4 and 5, respectively. y = 7.03 − 2.06x; r = 0.668, SEE 2.04.

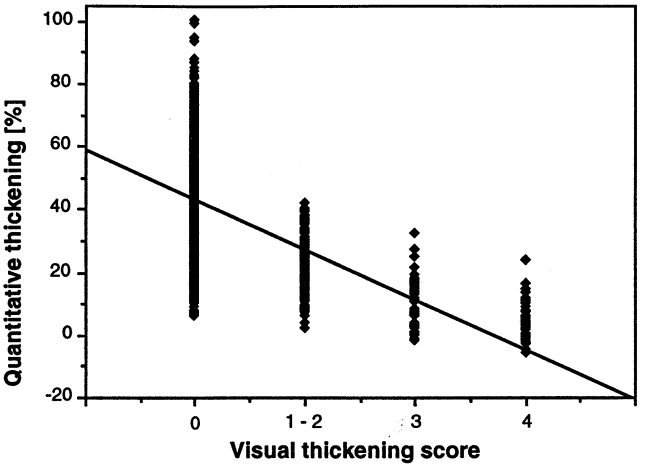

Figure 4. Quantitative segmental percent thickening versus visual thickening scores in the 1,296, 96, 101, 43 and 44 segments (total 1,580) with visual thickening scores of 0, 1, 2, 3 and 4, respectively. y = 43.01 − 15.96x; r = 0.550, SEE 15.56.

the initial estimate of thickness is corrected using the pseudo-constant myocardial volume constraint, measurements of thickening are accurate regardless of the camera used (dual- or triple-detector), the angular span of reconstructed data (180° or 360°) or amount of simulated thickening (0%, 33%, 50% or 100%). Similarly, measurements or simulated endocardial wall motion based on the corrected thickness are consistent across all system configurations and only slightly lower than the actual 3-mm and 6-mm displacements. In all measurements, the SD of the 360° images is smaller than that of the corresponding 180° images, owing to the known better uniformity of the 360° reconstruction. The SD of the triple-detector 180° images is smaller than that of the corresponding dual-detector 180° images, owing to the larger pixel size of the latter images.

Clinical patients. The algorithm was executed successfully in all 79 clinical patients studied—success being defined as the generation of endocardial and epicardial contours that matched the contours visually apparent in the images. Figure 3 and Table 2 compare visual motion scores and quantitative absolute motion in the 1,580 individual myocardial segments of the 79 patients (1,125, 295, 82, 43 and 35 segments with visual motion scores of 0, 1 to 2, 3, 4 and 5, respectively). Agreement was good by regression analysis (y = 7.03 − 2.06x, r = 0.668, SEE 2.04 mm) and fair by table analysis (kappa 0.433, exact agreement 72.6%). Figure 4 and Table 3 compare visual thickening scores and quantitative percent thickening in the same 1,580 individual myocardial segments (1,295, 195, 45 and 45 segments with visual thickening scores of 0, 1 to 2, 3 and 4, respectively). Again, agreement was fairly good by regression analysis (y = 43.01 − 15.96x, r = 0.550, SEE 15.56%) and fair by table analysis (kappa 0.408, exact agreement 74.7%). Of interest, 90.5% (950 of 1,050) of segments with a quantitative motion score >5 mm and 97.1% (1,007 of 1,037) of segments with a quantitative thickening score >30% were scored as normal by visual analysis.

Figure 5 compares, for each of the 79 patients studied, summed visual motion score and average quantitative motion. This global approach eliminates the possibility of error due to segmental misalignment between visual and automatic assessment. There were 21, 27, 8 and 23 patients with summed wall motion scores of 0 to 3, 4 to 8, 9 to 13 and >13, respectively. These categories were chosen based on our previous characterization of prognostically important degrees of myocardial hypoperfusion using a similar scoring system (21). The bar

Table 2. Agreement Table Relating Quantitative Motion and Visual Motion Scores in the 1,580 Segments Studied

Quantitative Motion	Visual Motion Scores				
	0	1–2	3	4	5
>5 mm	950	91	9	0	0
3–5 mm	162	135	22	3	7
1–3 mm	13	59	37	14	6
0–1 mm	0	6	9	12	8
<0 mm	0	4	5	14	14

Exact agreement 72.6%; kappa 0.433; $p < 0.05$.

Table 3. Agreement Table Relating Quantitative Thickening and Visual Thickening Scores in the 1,580 Segments Studied

Quantitative Thickening	Visual Thickening Scores			
	0	1–2	3	5
>30%	1,007	29	1	0
15–30%	264	125	11	2
5–15%	24	37	20	15
<5%	0	4	13	28

Exact agreement 74.7%; kappa 0.408; $p < 0.05$.

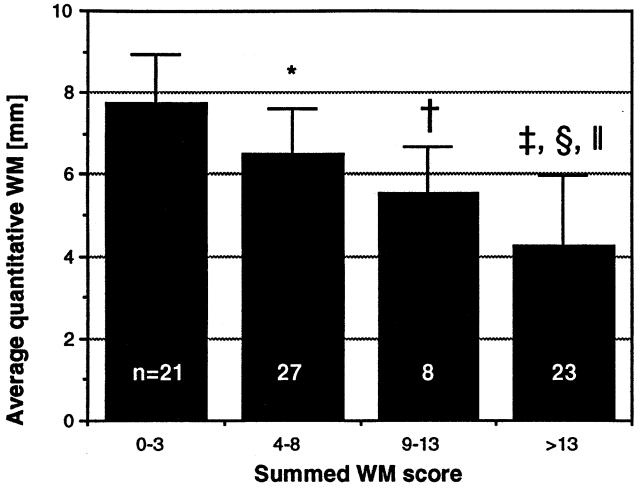

Figure 5. Summed wall motion (WM) score versus average quantitative wall motion in the 79 patients studied. *0 to 3 versus 4 to 8. †0 to 3 versus 9 to 13. ‡0 to 3 versus >13. §4 to 8 versus >13. $p < 0.05$ for each of these scores. ‖$p < 0.00001$ overall.

graph in Figure 5 demonstrates an inverse linear relation between summed motion score and average absolute motion in millimeters, with statistically significant differences between patients with summed scores of 0 to 3 vs. 4 to 8, 0 to 3 vs. 9 to 13, 0 to 3 vs. >13 and 4 to 8 vs. >13 ($p < 0.05$ for each) and overall ($p < 0.0001$). Analogously, Figure 6 compares summed visual thickening score and average quantitative percent thickening. There were 42, 13, 9 and 20 patients with summed wall thickening scores of 0 to 3, 4 to 8, 9 to 13 and >13, respectively. The bar graph in Figure 6 demonstrates an inverse linear relation between summed thickening score and average percent thickening, with statistically significant differences between patients with summed scores of 0 to 3 vs. 4 to 8, 0 to 3

Figure 6. Summed wall thickening (WT) score versus average quantitative percent wall thickening in the 79 patients studied. *0 to 3 versus 4 to 8. †0 to 3 versus 9 to 13. ‡0 to 3 versus >13. §4 to 8 versus >13. $p < 0.05$ for each of these scores. ‖$p < 0.00001$ overall.

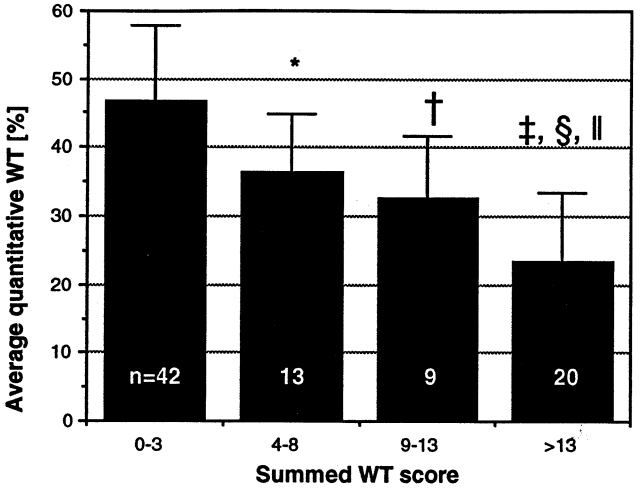

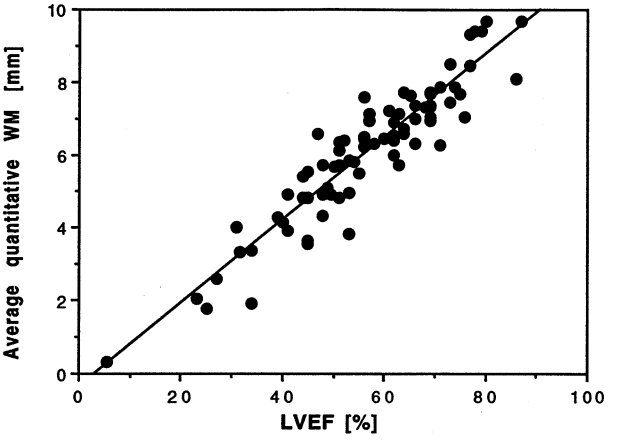

Figure 7. LVEF versus average quantitative myocardial wall motion (WM) in the 79 patients studied. $y = -0.37 + 0.11x$; $r = 0.929$, SEE 0.70.

vs. 9 to 13, 0 to 3 vs. >13 and 4 to 8 vs. >13 ($p < 0.05$ for each) and overall ($p < 0.0001$).

Figures 7 and 8 compare different quantitative global measurements of function generated by our automatic algorithm in the 79 patients studied. Figure 7 compares average quantitative motion with global quantitative LVEF, demonstrating extremely good agreement and a linear relation between these variables ($y = -0.37 + 0.11x$, $r = 0.929$, SEE 0.70 mm). Figure 8 compares average quantitative thickening with global quantitative LVEF, demonstrating extremely good agreement and a linear relation between them ($y = -11.27 + 0.88x$, $r = 0.959$, SEE 4.05%).

Discussion

This report describes the application of an automatic algorithm, capable of determining three-dimensional epicardial and endocardial surfaces from gated myocardial perfusion SPECT images, to the assessment of regional wall motion and

Figure 8. LVEF versus average quantitative percent myocardial wall thickening (WT) in the 79 patients studied. $y = -11.27 + 0.88x$; $r = 0.959$, SEE 4.05.

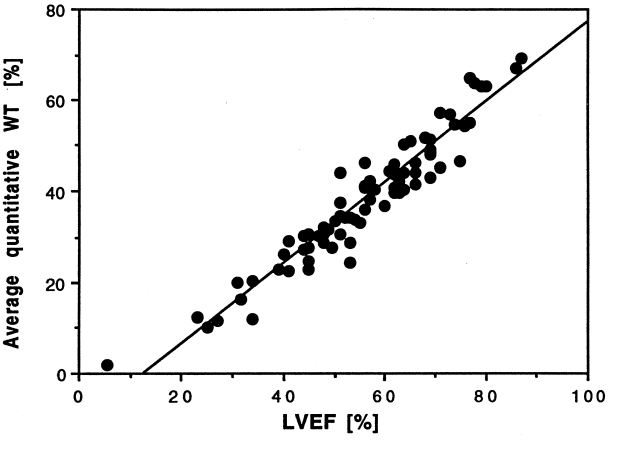

regional wall thickening. The algorithm operated successfully in all 79 patients studied. Significant correlation was observed between quantitative and visual assessments of regional wall motion and regional wall thickening. High correlations were also observed between the average quantitative motion in millimeters and the summed visual motion score, as well as between the average quantitative percent thickening and the summed visual thickening score. Finally, LVEF correlated extremely well with both summed wall thickening ($r = 0.959$) and summed wall motion ($r = 0.929$) scores. This latter result compares favorably with the correlation of $r = 0.83$ between LVEF and wall motion index reported by Ohsuzu et al. (23) for radionuclide ventriculography, as well as with the correlation of $r = 0.82$ between LVEF and end-systolic fractional shortening reported by Diamond et al. (24) for contrast ventriculography.

Heart translation and rotation. Extensive work with a variety of modalities has indicated the difficulty of correcting for translation and rotation of the heart in the assessment of regional ventricular function (3,5). The three-dimensional approach used in this study includes the translational motion of the heart in the measurement of endocardial motion, but eliminates the inaccuracies derived from the use of a fixed or floating reference system by adopting a three-dimensional extension of the coordinateless centerline method. This absolute measurement of motion will, in some cases, report paradoxic motion of healthy myocardial segments—for example, septal dyskinesia routinely found in patients after cardiac surgery (25); however, thickening measurements can easily help assess the functionality of the dyskinetic segments. Rotation of the heart during systole is not accounted for by our approach. It has been demonstrated, however, that this correction has very little effect on the assessment of the basal two-thirds of the LV (5,26), and its clinical relevance in assessing the distal one-third of the LV is uncertain (5). In routine clinical assessments by nearly all modalities, correction for rotation is not applied.

Limitations of the end-systolic/end-diastolic approach. Our approach uses end-diastolic and end-systolic measurements only. Wall motion abnormalities that may occur earlier (or later) than end-systole are therefore not detected by this technique. Figure 3 shows that our automatic algorithm assigned to the 35 dyskinetic segments (visual score of 5) a mean quantitative motion comparable to that of the 43 akinetic segments (visual score of 4), with a larger variance not directly ascribable to statistical considerations. It has been demonstrated that dyskinesia, as an example, in patients with myocardial infarction frequently occurs before the end of systole (27,28). Modifications of our approach could be made to account for abnormalities not detected at end-systole, but are not part of the present evaluation. This limitation may be exacerbated by our use of only 8 frames/cardiac cycle. We have previously examined the relation between 8- and 16-frame data and have shown little (and uniform) difference with respect to the assessment of LVEF (8). Whether assessing 16 frames as opposed to 8 frames will affect the assessment of regional ventricular function is currently under evaluation at our laboratory.

Myocardial thickness. Our technique is accurate in measuring myocardial wall thickening, although it is incapable of accurately measuring myocardial wall thickness (29). Myocardial thickness cannot theoretically be measured from nuclear medicine images, because such thickness is typically smaller than twice the full-width, half-maximum resolution of the reconstructed image (12). Resolution recovery using knowledge of the tomograph's point spread function has been attempted, but it has proved "computationally challenging," even for high resolution positron emission tomographic images (30).

Normal limits of regional function. It would be challenging to determine normal limits and criteria of abnormality based on absolute measurements of motion and thickening, as demonstrated by the fact that quantitative measurements corresponding to a visual score of 0 are not clearly separated from those corresponding to visual scores >0 (Fig 3 and 4). This potential limitation is by no means peculiar to nuclear medicine techniques. Echocardiographers have long been aware of it, as summarized by Katz et al. (5): "Normal segmental cavity shrinkage has been reported to vary from 0 percent (i.e., akynesis) to 100 percent and segmental wall thickening to vary from 0 to 150 percent." Analogously, magnetic resonance imaging (MRI) studies have reported a normal thickening range of 18% to 100% (31) and overall normal thickening of $48 \pm 28\%$ (32), the latter being a value consistent with our average normal thickening value of $43 \pm 17\%$, shown in Figure 4 for a visual score of 0. In contrast, a very interesting finding of our study is that a segment with quantitative motion >5 mm and thickening >30% has a 90.5% and 97.1% likelihood of being visually scored as normal, respectively. Our investigation is, at this stage, only concerned with whether one can measure absolute endocardial motion and myocardial thickening accurately and automatically; the issue of normal limits will be the goal of future research.

Reference standards of regional function. Finally, the standard against which our automatic quantitative regional function analysis was tested was expert visual assessment of regional wall motion and wall thickening. It has been stated that in contrast ventriculography "no gold standard exists for verifying the accuracy of wall motion measurements" (3), and the same consideration could apply to nuclear cardiology. It would have been desirable to validate the quantitative gated SPECT data against three-dimensional quantitative gated cardiac magnetic resonance imaging data. Difficulties connected with this approach range from the organizational (MRI and SPECT acquisitions must be performed in close temporal proximity and with the patient in the same loading conditions) to the technical (true three-dimensional acquisition of high quality cine MRI data encompassing the entire LV is difficult using current instrumentation). These difficulties are probably responsible for the existence of only two published studies, to date, comparing regional myocardial function by gated MRI and gated perfusion SPECT—one conducted in semiquantita-

tive fashion on four patients (33) and the other visually comparing two-dimensional regional function in 24 patients (34). Protocols for validation of quantitative SPECT regional wall motion and thickening compared with MRI (as well as for the assessment of the incremental value of SPECT function over perfusion alone) are currently under investigation at our institution.

Conclusions. We developed an automatic algorithm for the quantitative measurement of regional myocardial wall motion and wall thickening from three-dimensional gated Tc-99m sestamibi SPECT images, and we tested it using a "variable thickness" heart phantom. We also compared the quantitative algorithm's output to visual segmental scores in 79 clinical patients with a wide range of ejection fractions and regional function. The algorithm is accurate and may be the first automatic technique for the quantitative three-dimensional assessment of regional ventricular function in cardiology. In its current implementation on a low cost, off-the-shelf computer platform, the algorithm automatically generated numeric measurements of LVEF, regional wall motion and regional wall thickening in 20 s for each eight-frame gated SPECT study.

We thank Rory Hachamovitch, MD, Hosen Kiat, MD and Mark Hyun for their assistance.

References

1. Shiina A, Tajik AJ, Smith HC, Lengyel M, Seward JB. Prognostic significance of regional wall motion abnormality in patients with prior myocardial infarction: a prospective correlative study of two-dimensional echocardiography and angiography. Mayo Clin Proc 1986;61:254–62.
2. Kennedy JW, Kaiser GC, Fisher LD, et al. Clinical and angiographic predictors of operative mortality from the collaborative Coronary Artery Surgery Study (CASS). Circulation 1981;63:793–802.
3. Sheehan F. Principles and practice of contrast ventriculography. In: Marcus ML and Braunwald E, editors. Marcus Cardiac Imaging: A Companion to Braunwald's Heart Disease. Philadelphia: W.B. Saunders, 1996:164–87.
4. Murphy P, Port S. Radionuclide evaluation of left ventricular function. In: Sandler MP, editor. Diagnostic Nuclear Medicine. Baltimore: Williams & Wilkins, 1995;403–42.
5. Katz A, Force T, Folland E, Aebischer N, Sharma S, Parisi A. Echocardiographic assessment of ventricular systolic function. In: Marcus ML and Braunwald E, editors. Marcus Cardiac Imaging: A Companion to Braunwald's Heart Disease. Philadelphia: W.B. Saunders, 1996:297–324.
6. van der Wall EE, Vliegen HW, de Roos A, Bruschke AV. Magnetic resonance imaging in coronary artery disease. Circulation 1995;92:2723–39.
7. Mousseaux E, Gaux JC. Ultrafast computed tomography of the heart. Curr Opin Radiol 1992;4:34–40.
8. Germano G, Kiat H, Kavanagh PB, et al. Automatic quantification of ejection fraction from gated myocardial perfusion SPECT. J Nucl Med 1995;36:2138–47.
9. Mazzanti M, Germano G, Kiat H, et al. Identification of severe and extensive coronary artery disease by automatic measurement of transient ischemic dilation of the left ventricle in dual isotope myocardial perfusion SPECT. J Am Coll Cardiol 1996;27:1612–20.
10. Everaert H, Franken P, Flamen P, Momen A, Bossuyt A. Left ventricular volumes and ejection fraction from gated SPECT myocardial perfusion studies [abstract]. J Nucl Cardiol 1997;4(1 Pt 2):S102.
11. Cooke CD, Garcia EV, Cullom SJ, Faber TL, Pettigrew RI. Determining the accuracy of calculating systolic wall thickening using a fast Fourier transform approximation: a simulation study based on canine and patient data. J Nucl Med 1994;35:1185–92.
12. Hoffman EJ, Huang SC, Phelps ME. Quantitation in positron emission computed tomography: 1. Effect of object size. J Comput Assist Tomogr 1979;3:299–308.
13. Sheehan FH, Dodge HT, Mathey D, Brown BG, Bolson EL, Mitten S. Application of the centerline method: analysis of change in regional left ventricular wall motion in serial studies. Comput Cardiol 1983:97–100.
14. Faber TL, Akers MS, Peshock RM, Corbett JR. Three-dimensional motion and perfusion quantification in gated single-photon emission computed tomograms. J Nucl Med 1991;32:2311–7.
15. Germano G, Kavanagh PB, Chen J, et al. Operator-less processing of myocardial perfusion SPECT studies. J Nucl Med 1995;36:2127–32.
16. Digby WM. Techniques for improved accuracy and precision using modular detector systems for positron emission tomography [dissertation]. Los Angeles (CA): University of California Los Angeles, 1991.
17. Berman DS, Kiat H, Friedman JD, et al. Separate acquisition rest thallium-201/stress technetium-99m sestamibi dual-isotope myocardial perfusion single-photon emission computed tomography: a clinical validation study. J Am Coll Cardiol 1993;22:1455–64.
18. Germano G, Van Train K, Garcia E, et al. Quantitation of myocardial perfusion with SPECT: current issues and future trends. In: Zaret BL, Beller G, editors. Nuclear Cardiology: State of the Art and Future Directions. St. Louis: Mosby, 1993:77–88.
19. Garcia EV, Cooke CD, Van Train KF, et al. Technical aspects of myocardial SPECT imaging with technetium-99m sestamibi. Am J Cardiol 1990;66:23E–31E.
20. Germano G, Kavanagh PB, Berman DS. Effect of the number of projections collected on quantitative perfusion and left ventricular ejection fraction measurements from gated myocardial perfusion single-photon emission computed tomographic images. J Nucl Cardiol 1996;3:395–402.
21. Hachamovitch R, Berman DS, Kiat H, et al. Gender-related differences in clinical management after exercise nuclear testing. J Am Coll Cardiol 1995;26:1457–64.
22. Fleiss JL. Statistical Methods for Rates and Proportions. New York: Wiley, 1973.
23. Ohsuzu F, Boucher CA, Newell JB, et al. Relation of segmental wall motion to global left ventricular function in acute myocardial infarction. Am J Cardiol 1983;51:1275–81.
24. Diamond GA, Vas R, Forrester JS, et al. The influence of bias on the subjective interpretation of cardiac angiograms. Am Heart J 1984;107:68–74.
25. De Nardo D, Caretta Q, Mercanti C, et al. Effects of uncomplicated coronary artery bypass graft surgery on global and regional left ventricular function at rest: study by equilibrium radionuclide angiocardiography. Cardiology 1989;76:285–92.
26. Mirro MJ, Rogers EW, Weyman AE, Feigenbaum H. Angular displacement of the papillary muscles during the cardiac cycle. Circulation 1979;60:327–33.
27. Sniderman AD, Marpole D, Fallen EL. Regional contraction patterns in the normal and ischemic left ventricle in man. Am J Cardiol 1973;31:484–9.
28. Weyman AE, Franklin TD Jr, Hogan RD, et al. Importance of temporal heterogeneity in assessing the contraction abnormalities associated with acute myocardial ischemia. Circulation 1984;70:102–12.
29. Williams KA, Lang RM, Reba RC, Taillon LA. Comparison of technetium-99m sestamibi–gated tomographic perfusion imaging with echocardiography and electrocardiography for determination of left ventricular mass. Am J Cardiol 1996;77:750–5.
30. Jones T. The imaging science of positron emission tomography. Eur J Nucl Med 1996;23:807–13.
31. Sechtem U, Sommerhoff BA, Markiewicz W, White RD, Cheitlin MD, Higgins CB. Regional left ventricular wall thickening by magnetic resonance imaging: evaluation in normal persons and patients with global and regional dysfunction. Am J Cardiol 1987;59:145–51.
32. Pflugfelder PW, Sechtem UP, White RD, Higgins CB. Quantification of regional myocardial function by rapid cine MR imaging. Am J Roentgenol 1988;150:523–9.
33. Faber TL, Stokely EM, Peshock RM, Corbett JR. A model-based four-dimensional left ventricular surface detector. IEEE Trans Med Imaging 1991;10:321–9.
34. Anagnostopoulos C, Laney R, Pennell D, Proukakis H, Underwood R. A comparison of resting images from two myocardial perfusion tracers. Eur J Nucl Med 1995;22:1029–34.